Clays and Clay Minerals, Vol. 38, No. 4, 415–425, 1990.

HYDROTHERMAL REACTIVITY OF MIXED-LAYER KAOLINITE/SMECTITE: EXPERIMENTAL TRANSFORMATION OF HIGH-CHARGE TO LOW-CHARGE SMECTITE

D. PROUST[1], J. LECHELLE,[2] A. LAJUDIE,[2] AND A. MEUNIER[1]

[1] Laboratoire de Pétrologie des Alterérations Hydrothermales
Université de Poitiers, 86022 Poitiers Cedex, France

[2] Commissariat à l'Energie Atomique, DRDD/SESD
92260 Fontenay-aux-Roses, France

Abstract—A mixed-layer kaolinite/smectite (K/S) containing trace amounts of quartz, discrete kaolinite, goethite-hematite, and calcite was hydrothermally reacted with deionized water at 150°, 200°, and 250°C for 1 to 12 months. The starting K/S contained 50% smectite consisting of 15% low-charge and 35% high-charge layers. The X-ray powder diffraction and chemical analyses of the reacted products indicated a progressive reaction from high-charge to low-charge smectite as a function of time and temperature. The reaction reached completion after 4 months at 250°C, at which point high-charge smectite layers entirely reacted to low-charge smectite layers, the latter maintaining a constant proportion of about 90% for longer run durations. For long reaction times, discrete kaolinite totally reacted, whereas quartz showed only partial dissolution and iron oxides remained stable. Thus, the reaction of high-charge to low-charge smectite layers may be expressed as: high-charge smectite + kaolinite (both interstratified and discrete component) + quartz → low-charge smectite.

Key Words—Cation-exchange capacity, Hydrothermal transformation, Kaolinite/smectite, Layer charge, Smectite, X-ray powder diffraction.

INTRODUCTION

Many workers have observed that dioctahedral smectites are not stable at temperatures >75°–100°C under diagenetic conditions. The most detailed studies of smectite reactivity as a function of temperature have focused on the smectite-to-illite conversion in potassium-rich environments via intermediate mixed-layer illite/smectite (I/S). Studies of natural, low-temperature geological environments (see, e.g., Hower *et al.*, 1976; Inoue *et al.*, 1978; Velde and Brusewitz, 1982; Inoue and Utada, 1983; Ramseyer and Boles, 1986) as well as laboratory experiments (Eberl and Hower, 1976; Eberl, 1978; Roberson and Lahann, 1981; Howard and Roy, 1985), suggest that smectite illitization operates through tetrahedral Al-for-Si and octahedral Mg-for-Al ionic substitutions within the 2:1 layer. These ionic substitutions create an increasing negative layer charge with the formation of high-charge smectite and K-fixation in the interlayer sites (Howard, 1981; Howard and Roy, 1985).

Illitization reactions have been formally expressed as:

(1) Smectite + Al^{3+} + K^+ → illite + Si^{4+}, if solid-phase transformation is assumed (Hower *et al.*, 1976); and

(2) Smectite + K^+ → illite + Si^{4+}, if smectite dissolution is assumed to supply Al for illite crystallization (Boles and Franks, 1979).

These two reactions lead to the release of Si to solution. A recent study of I/S stability in a natural, low-temperature hydrothermal environment (Bouchet *et al.*, 1988) suggested that the high-charge smectite component of the I/S reacted to form: (1) illite, if external K was supplied (i.e., high-charge smectite + K^+ → illite) or (2) low-charge smectite, if external Si was supplied (i.e., high-charge smectite + Si^{4+} → low-charge smectite). The second reaction induces a marked increase in the cation-exchange capacity (CEC) of the clay material. The main purpose of this paper was therefore to study further the reaction of high-charge to low-charge smectite under experimental alteration conditions. To avoid uncontrolled smectite illitization, the following constraints were imposed on the experiments: (1) the starting expandable clay material was free of illite, either as a discrete clay mineral or as a component of a mixed-layer clay mineral, and (2) alteration solutions were potassium-free.

Hydrothermal runs were therefore conducted using a mixed-layer kaolinite/smectite (K/S) as the starting clay material, run durations of 1 to 12 months, temperatures of 150°, 200°, and 250°C, and deionized water as the alteration solution.

MATERIAL AND EXPERIMENTAL METHODS

Material

The starting clay for the hydrothermal runs was obtained from the Sparnacian Argiles Plastiques Formation in the northwestern part of the Paris Basin (Vexin area). These clays occur in highly weathered

continental deposits inherited from the erosion of Paleocene weathered profiles, which had developed on late Cretaceous (Senonian) chalk-flint. Mixed-layer K/S is the dominant species (Thiry *et al.,* 1977; Thiry, 1981) with major smectite component (Lucas *et al.,* 1974; Brindley *et al.,* 1983; Coulon, 1987).

Experimental procedure

For each run, 20 g of a slurry containing a 1.3:1 deionized water-to-clay ratio was loaded into sealed, gold-plated capsules and heated in autoclaves at 150°, 200°, and 250°C for from 1 to 12 months. The internal pressure was the steam-saturated H_2O_{liquid} pressure at the temperature of experiment (respectively, 4.76, 15.54, and 39.73 bars at 150°, 200°, and 250°C). Upon completion of a run, the samples were quenched, and the solid products were separated from solutions by centrifugation and analyzed by the following methods.

X-ray powder diffraction

X-ray powder diffraction (XRD) patterns of all samples were recorded using a Philips PW 1730 X-ray diffractometer (40 kV, 40 mA) with Fe-filtered CoKα radiation. A proportional detector (Philips 1965/60) was used with a 0.1° divergence slit, a 1° receiving slit, and a continuous scanning speed of 0.5°2θ/min. A linear localization detector of X-rays (Elphyse) was used in place of a proportional detector if higher resolution (peak/background ratio) was needed for weak reflections. The X-ray incident beam was focused using a collimator 0.8 mm in diameter, which gave a 8 mm × 2 mm irradiated area at 2°2θ (Rassineux *et al.,* 1988). Samples were prepared as natural, Mg-saturated, and K-saturated suspensions, pipeted onto glass slides, air dried, and solvated with ethylene glycol (EG) using the liquid technique of Środoń (1980). Additional Ca-saturations were made of the K-exchanged samples in order to estimate the proportion of high-charge to low-charge smectite layers. Low-charge layers maintain their expandability with EG, but high-charge layers collapse after K-saturation and do not reexpand after Ca-saturation and EG solvation (Howard and Roy, 1985).

The starting clay material displayed poorly resolved, high-order basal XRD reflections (indicative of a few layers in the crystallite), which did not allow precise d-value calculations. Under these conditions, the identification of the mixed-layer minerals (ordering type and component ratio) was made by comparing the positions of the first two basal reflections with those computed with variable layer ratio and ordering type using the Newmod program available from R. C. Reynolds, Department of Earth Sciences, Dartmouth College, Hanover, New Hampshire. Estimated layer ratios are thought to be accurate within ±5% (Bouchet *et al.,* 1988).

Chemical analyses

Chemical analyses of pressed pellets of the starting and reacted products were obtained using a Cameca MS 46 electron microprobe equipped with an EGG Ortec energy-dispersive X-ray analysis system. The analytical procedure was that recommended by Velde (1984) for clay minerals: 120-s counting time, 15-kV acceleration potential, 1-nA sample current, and 5-μm spot diameter. The cation-exchange capacities (CECs) were measured by the ammonium acetate method of Jackson (1958) at pH 7.

The amount of quartz in the clay material was estimated to be 6.7 ± 0.4%, using the triacid attack method (Voinovitch *et al.,* 1962); the calcite content was estimated to be 2 ± 0.2% using the calcimeter method. The iron oxide content was estimated using ^{57}Fe Mössbauer spectroscopy; spectra were recorded at room temperature, 77, 4.2, and 1.5 K.

RESULTS AND DISCUSSION

Mineralogy of the starting clays

X-ray powder diffraction. XRD patterns obtained with proportional and linear localization detectors of powder sample exhibited trace amounts of quartz (4.25 and 3.35 Å), goethite (4.18 Å), calcite (3.04 Å), and discrete (non-interstratified) kaolinite (7.19, 4.46, and 3.56 Å). XRD patterns recorded with the linear detector in the 64°–76°2θ region showed two 060 reflections at 1.490 for the discrete kaolinite and 1.494 Å for a coexisting dioctahedral clay mineral (Figure 1). No reflection was observed in the 1.53–1.55-Å region that could be assigned to a trioctahedral clay mineral (Brown and Brindley, 1980).

XRD patterns obtained with proportional and linear detectors of oriented samples are shown in Figure 2. XRD traces of the Mg sample yielded peaks at 14.66 and 7.19 Å, which are, respectively, the 001 reflections of a 14-Å clay mineral and discrete kaolinite. EG solvation did not shift the 7.19-Å reflection of the discrete kaolinite, whereas the 14.66-Å reflection shifted to 17.10 Å and an additional reflection appeared at 8.20 Å. The 17.10-Å reflection is typical for expandable smectite layers containing two interlayers of EG molecules (Čičel and Machajdik, 1981).

This smectite determination is supported by the collapse of the layers at 9.51 and 9.45 Å after heating at 300°C and 550°C for 2 hr. These thermal treatments preclude the possibility of a chlorite component (discrete or interstratified phase), inasmuch as no reflection was observed in the 10–24-Å range.

The XRD patterns of glycolated Mg-smectite layers were distinct from those of pure smectite: (1) The 001 reflection at 17.10 Å after EG solvation showed a pronounced asymmetry, having a high saddle in the low-angle region, which did not match with the symmetrical, low-background 001 reflection of a pure gly-

https://doi.org/10.1346/CCMN.1990.0380411 Published online by Cambridge University Press

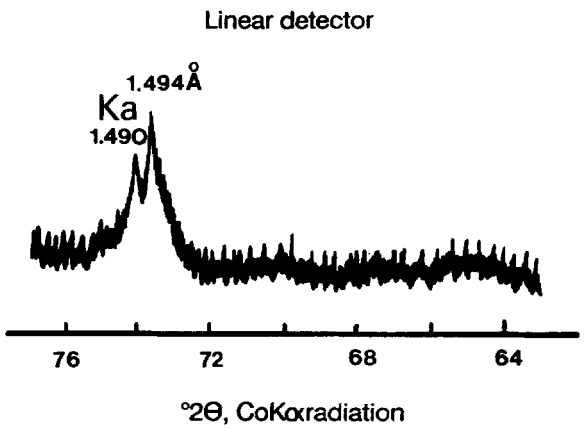

Figure 1. X-ray powder diffraction pattern of the starting clay material in the 060 reflection region (unoriented preparation). Ka = kaolinite.

colated smectite. (2) The 8.20-Å reflection obtained after glycolation of the sample did not match with the rational d(002) value of a pure smectite, which should be at 8.55 Å as the second order of the 17.10-Å 001 reflection. These two observations suggest a random interstratification (no "superorder" basal reflection was observed) of the smectite component with another clay mineral (Reynolds and Hower, 1970). The thermal treatments and the 060 reflection data preclude the possibility of a chlorite component, either as a component of interstratification or as a discrete phase; hence, the only possible interstratifications of the dioctahedral smectite with another clay mineral are illite/smectite or kaolinite/smectite.

The computed diffractograms of glycolated, random I/S (Reynolds, 1980), show that the $d[(001)_{illite}/(002)_{smectite}]$ values range from 10.16 Å for 100% illite to 8.52 Å for 100% glycolated smectite; thus, the 8.20-Å reflection of the studied mixed layer clay cannot be assigned to a mixed-layer I/S. The best fit between the glycolated experimental and computed diffractograms was obtained by simulating a random (R=0) mixed-layer K/S with a value of N = 10 and varying proportions of expandable layers. A diagram giving the percentage of expandable smectite layers within the K/S as a function of $d[(001)_{kaolinite}/(002)_{smectite}]$ was then constructed from the simulated patterns (Figure 3). A plot of the experimental $d[(001)_{kaolinite}/(002)_{smectite}]$ value of the unreacted, glycolated sample into this diagram gives 50% maximum expandability (% Tot. Sm., Table 1). The EG solvation of the K-Ca-exchanged sample shifted the $001_{kaolinite}/002_{smectite}$ composite reflection from 8.20 to 7.75 Å, indicating the collapse of a part of the expandable smectite layers, i.e., high-charge smectite layers. Thus, a plot of the new $d[(001)_{kaolinite}/(002)_{smectite}]$ values on Figure 3 will give the proportion of expandable low-charge smectite in the K/S, the proportion of

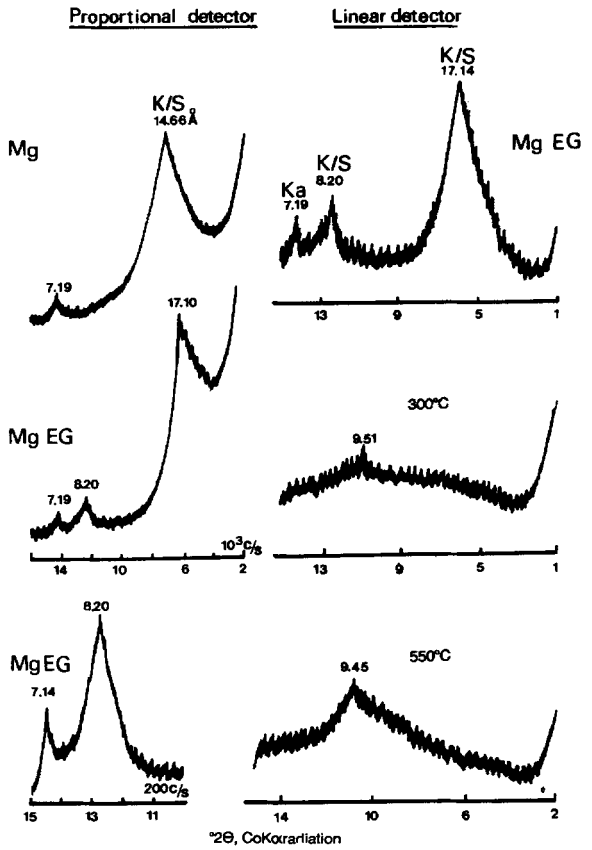

Figure 2. X-ray powder diffraction patterns of the starting clay material (oriented preparation). Mg = magnesium saturated; Mg EG = magnesium saturated and glycolated; 300°C, 550°C = heated for 2 hr at 300°C or 550°C; Ka = kaolinite; K/S = mixed-layer kaolinite/smectite.

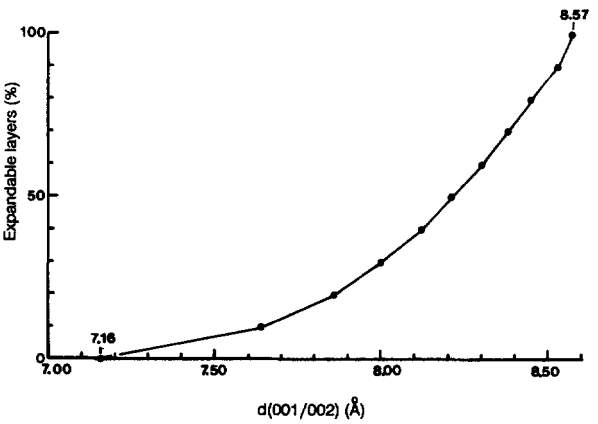

Figure 3. Computed quantification curve of the percentage of expandable layers in the mixed-layer kaolinite/smectite as a function of d(001/002) spacings. Patterns were calculated with a total number of layers N = 10 in the crystallite; the smectite component was defined as: d(001) = 17 Å, 0.2 Fe atom for $O_{10}(OH)_2$ anion content, Mg as interlayer cation.

https://doi.org/10.1346/CCMN.1990.0380411 Published online by Cambridge University Press

Table 1. Estimation of the smectite content in starting mixed-layer kaolinite/smectite using X-ray powder diffraction data.

Maximum expandability		Low-charge expandability		High-charge percentage: % HC. Sm.
d(001/002) 8.20 Å	% Tot. Sm. 50%	d(001/002) 7.75 Å	% LC. Sm. 15%	% Tot. Sm. − % LC. Sm. 35%

% Tot. Sm. = total percentage of smectite; % LC. Sm. = percentage of low-charge smectite; % HC. Sm. = percentage of high-charge smectite.

high-charge smectite layers (% HC. Sm.) being obtained by: % high-charge smectite = % total smectite − % low-charge smectite. The results (Table 1) give maximum values of 15% low-charge and 35% high-charge smectite layers.

Chemical composition of smectite layers. Electron microprobe analyses of the starting clay material are given in Table 2. Mössbauer data indicated that all iron was in the Fe^{3+} oxidation state with the following partition: 3% as hematite (α-Fe_2O_3), 70% as goethite (α-FeOOH), and 27% entering clay mineral structures. The correction procedure for the iron oxide contents was the following: (1) The total Fe_2O_3 content was converted to millimoles of Fe^{3+} and distributed among hematite, goethite, and clay minerals using the partition values. (2) Hematite and goethite contents were then calculated using molecular weights of each species; Fe_2O_3 allocated to hematite and goethite (conversion of FeOOH to Fe_2O_3) was then subtracted from the total Fe_2O_3 to obtain the amount of Fe_2O_3 in the clay mineral. The same procedure was used to correct for 2% calcite; the quartz content obtained from the triacid attack (6.7%) was directly subtracted from the total SiO_2. These corrected analyses thus represent the chemical composition of the mixture: mixed-layer K/S + discrete kaolinite. In these conditions, the calculation of a structural formula representing the mixed-layer K/S seems unrealistic.

This two-phase assemblage was graphically represented on the M^+–4Si–R^{2+} diagram (Figure 4) of Meunier and Velde (1989), where M^+ = 2Ca + Na + K, 4Si = Si/4, R^{2+} = Mg + Mn. A mixed-layer K/S should plot between the 4Si pole (pure kaolinite) and the dioctahedral smectite field, depending on the proportion of each component.

Natural dioctahedral smectites plot in a chemical domain bounded by two composition lines (Figure 4):

1. The $mo_{0.33}$–$mo_{0.66}$ composition line with ideal low- and high-charge montmorillonite end-members:

$mo_{0.33}$: $[Si_4]O_{10}[(Al,Fe^{3+})_{1.67}R^{2+}_{0.33}](OH)_2M^+_{0.33}$ and
$mo_{0.66}$: $[Si_4]O_{10}[(Al,Fe^{3+})_{1.34}R^{2+}_{0.66}](OH)_2M^+_{0.66}$.

Intermediate compositions between these two poles are governed by the $R^{2+}M^+ \rightarrow Al^{VI}$ substitution.

2. The $be_{0.33}$–$be_{0.66}$ composition line with ideal low- and high-charge beidellite end-members:

Table 2. Electron microprobe analyses (wt. %) of starting clay material.

	Bulk chemical analyses											
												Mean
SiO_2	45.99	46.81	42.09	47.17	44.22	42.61	42.00	42.09	47.17	40.83	45.46	44.22
Al_2O_3	25.36	26.10	23.50	26.51	23.66	22.72	23.60	23.50	26.51	22.90	24.67	24.46
MnO	0.34	0.61	0.49	0.35	0.11	—	—	0.49	0.35	0.07	0.18	0.27
MgO	1.16	0.88	0.83	1.11	0.69	0.77	1.16	0.83	1.11	0.74	0.89	0.92
CaO	2.93	2.87	2.88	2.80	2.80	2.38	2.51	2.88	2.80	2.28	2.47	2.69
Na_2O	0.76	0.16	—	0.43	—	0.37	0.21	—	0.43	0.47	0.61	0.31
K_2O	0.40	0.44	0.70	0.14	—	0.40	0.27	0.70	0.14	0.06	0.07	0.30
TiO_2	2.20	1.75	2.79	2.90	1.32	1.40	1.59	1.49	1.66	1.27	1.54	1.81
Fe_2O_3	7.24	6.81	6.83	7.27	5.96	8.70	6.47	6.83	7.27	10.79	7.50	7.42
	Chemical analyses corrected for quartz (6.7%), calcite (2%), goethite (% goet.), and hematite (% hem.)											
% Goet.	5.63	5.30	5.32	5.66	4.64	6.78	5.04	5.32	5.66	8.40	5.84	5.78
% Hem.	0.22	0.20	0.20	0.22	0.18	0.26	0.19	0.20	0.22	0.32	0.22	0.22
SiO_2	39.29	40.11	35.39	40.47	37.52	35.91	35.30	35.39	40.47	34.13	38.76	37.52
Al_2O_3	25.36	26.10	23.50	26.51	23.66	22.72	23.60	23.50	26.51	22.90	24.67	24.46
MnO	0.34	0.61	0.49	0.35	0.11	—	—	0.49	0.35	0.07	0.18	0.27
MgO	1.16	0.88	0.83	1.11	0.69	0.77	1.16	0.83	1.11	0.74	0.89	0.92
CaO	1.81	1.75	1.76	1.68	1.68	1.26	1.39	1.76	1.68	1.16	1.35	1.57
Na_2O	0.76	0.16	—	0.43	—	0.37	0.21	—	0.43	0.47	0.61	0.31
K_2O	0.40	0.44	0.70	0.14	—	0.40	0.27	0.70	0.14	0.06	0.07	0.30
TiO_2	2.20	1.75	2.79	2.90	1.32	1.40	1.59	1.49	1.66	1.27	1.54	1.81
Fe_2O_3	1.95	1.84	1.84	1.96	1.61	2.35	1.75	1.84	1.96	2.91	2.02	2.00

https://doi.org/10.1346/CCMN.1990.0380411 Published online by Cambridge University Press

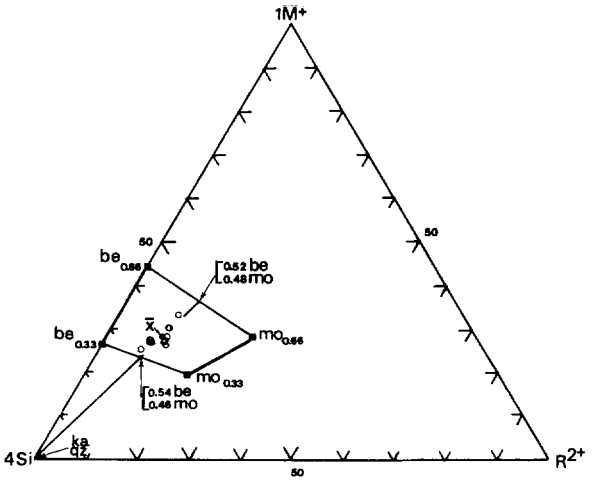

Figure 4. Plots of the corrected microprobe analyses of the starting clay material in the M^+–4Si–R^{2+} diagram; be = beidellite; mo = montmorillonite; Ka = kaolinite; Qz = quartz; 0.52 be–0.48 mo = % of end-members beidellite and montmorillonite in the smectite component of the mixed-layer kaolinite/smectite; $\bar{X}$ = mean value of microprobe analyses.

$be_{0.33}$: $[Si_{3.67}Al_{0.33}]O_{10}[(Al,Fe^{3+})_2](OH)_2M^+_{0.33}$ and $be_{0.66}$: $[Si_{3.34}Al_{0.66}]O_{10}[(Al,Fe^{3+})_2](OH)_2M^+_{0.66}$.

Intermediate compositions between these two poles are governed by the degree of Al^{IV} $M^+ \rightarrow Si^{IV}$ substitution with R^{2+}=0.

The corrected microprobe analyses of the studied sample, plotted on a M^+–4Si–R^{2+} diagram (Figure 4), are, of course, in the line with the 4Si pole (kaolinite) and intersect the $be_{0.33}$–$mo_{0.33}$ and $be_{0.66}$–$mo_{0.66}$ lines, indicating that each low-charge and high-charge smectite component is neither pure beidellite nor montmorillonite, but has an intermediate composition in the beidellite-montmorillonite solid solution series. The development of the layer charge within each component was thus produced by simultaneous $Al^{IV} \rightarrow Si^{IV}$ and $R^{2+} \rightarrow Al^{VI}$ substitutions.

The chemical composition of the low-charge and high-charge smectite layers can be tentatively estimated using the percentages of beidellite and montmorillonite obtained from the intersected $be_{0.33}$–$mo_{0.33}$ and $be_{0.66}$–$mo_{0.66}$ lines (Figure 4) and the composition of each end-member. The resulting structural formulae are:

Low-charge smectite: $[Si_{3.82}\ Al_{0.18}]\ O_{10}\ [(Al,Fe^{3+})_{1.85} \cdot R^{2+}_{0.15}](OH)_2M^+_{0.33}$, and

High-charge smectite: $[Si_{3.66}\ Al_{0.34}]\ O_{10}\ [(Al,Fe^{3+})_{1.68} \cdot R^{2+}_{0.32}](OH)_2\ M^+_{0.66}$.

Considering that alkaline earth elements do not enter the kaolinite structure, the electron microprobe analyses (Table 2) indicate that the negative layer charges of the smectite components in the mixed-layer K/S are

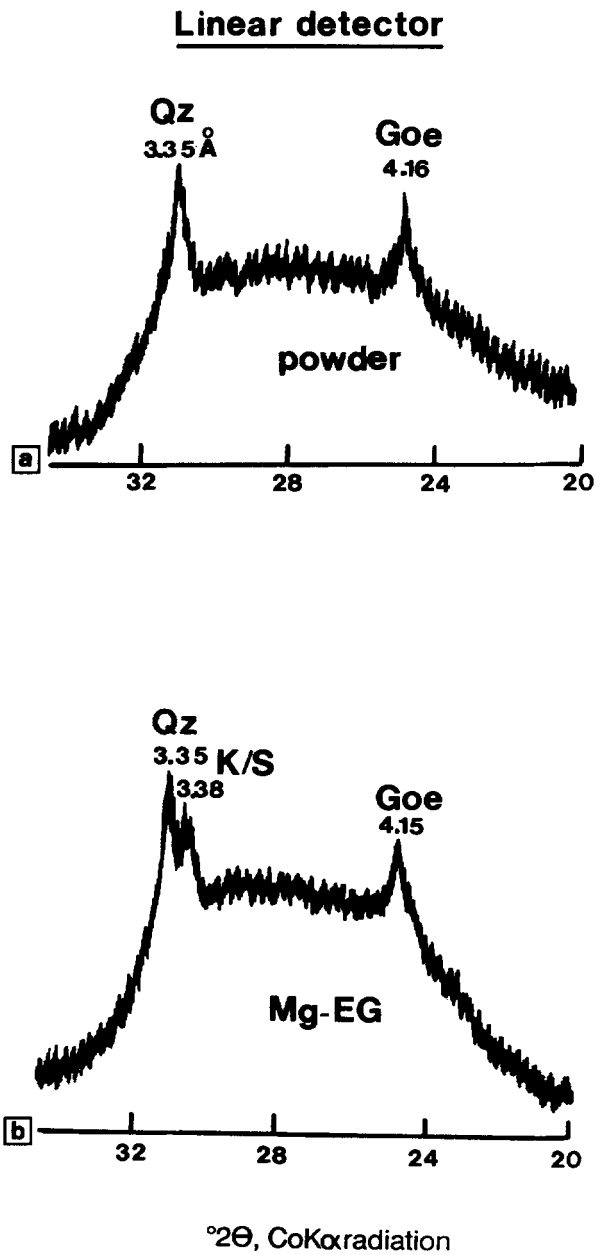

Figure 5. X-ray powder diffraction patterns of the clay material after reaction at 250°C for 12 months. (a) unoriented preparation; (b) oriented preparation, saturated with magnesium and glycolated. Goe = goethite; K/S = mixed-layer kaolinite/smectite; Qz = quartz.

mainly balanced by calcium in interlayer sites. The CEC value of 63.80 meq/100 g, however, is lower than the CEC of pure smectite, which ranges from 100 to 150 meq/100 g (Hower and Mowatt, 1966; Nadeau and Bain, 1986; Środoń *et al.*, 1986).

From this initial identification, the starting clay material apparently fullfills the following requirements to

https://doi.org/10.1346/CCMN.1990.0380411 Published online by Cambridge University Press

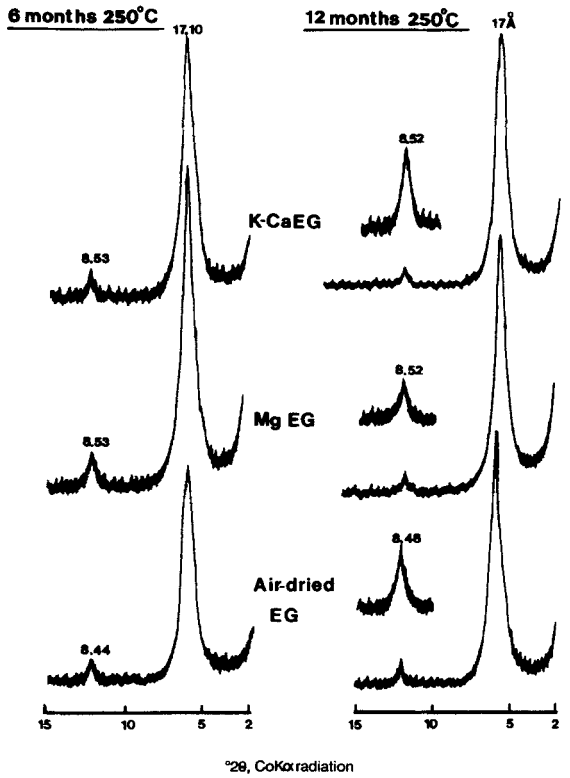

Figure 6. X-ray powder diffraction patterns of the clay material after reaction at 250°C for 12 months, oriented preparation. K-Ca-EG = K-saturated, air-dried, saturated with Ca, and glycolated; Mg-EG = magnesium saturated and glycolated.

test the high-charge to low-charge smectite reaction: (1) lack of illitic phase in the bulk sample and high smectite content in the mixed-layer K/S; and (2) dominant high-charge smectite layers in the starting mixed-layer K/S.

Mineralogy of the hydrothermally reacted clays

X-ray powder diffraction and CEC data. Representative XRD patterns of the clay material after its reaction at 250°C for 6 and 12 months with deionized water are illustrated in Figures 5 and 6. The powder pattern recorded after 12 months at 250°C with the linear detector (Figure 5a) shows the marked decrease of the 3.35-Å quartz reflection, the disappearance of the 3.04-Å calcite reflection, and the stability of the 4.16-Å goethite reflection compared with the unreacted sample (Figure 1). These observations indicate that calcite and quartz were not stable phases under the experimental alteration conditions and reacted to a different degree as a function of time and temperature. The complete reaction of calcite was obtained after 4 months at 250°C, whereas quartz dissolution was incomplete and began after about 1 month at 250°C.

The XRD patterns of the oriented glycolated samples (Figure 6) show the complete destabilization of the discrete kaolinite (i.e., no 7.19-Å kaolinite reflection), as previously observed for the 4 month-250°C run. Simultaneously, the $d[(001)_{kaolinite}/(002)_{smectite}]$ values of the K/S increased, respectively, from 8.20 Å in the unreacted sample (Figure 2) to 8.53 and 8.52 Å after 6 and 12 months at 250°C.

The proportions of total smectite layers estimated from the d(001/002) spacings are listed in Table 3. Figure 7a, a plot of maximum expandability (% Tot. Sm.) vs. time and temperature, clearly indicates that the hydrothermal alteration of the K/S results in the increase of the total smectite proportion with time and temperature. The starting K/S (originally 50% maximum expandability) reacted strongly in the first month of alteration at 250°C, with a rapid increase of total smectite proportion (82%) as a function of temperature. Longer runs led to the stabilization of the smectite

Table 3. Estimation of the smectite content in reacted mixed-layer kaolinite/smectite using X-ray powder diffraction data and cation-exchange capacities.

Run with deionized water	Mg-EG: % Tot. Sm.		K-Ca-EG: % LC. Sm.			
	d(001/002) (Å)	% Tot. Sm.	d(001/002) (Å)	% LC. Sm.	% HC. Sm.	CEC (meq/100 g)
Unreacted	8.20	50	7.75	15	35	63.80
1 month 200°C	8.29	59	7.86	19	40	68.60
1 month 250°C	8.47	82	8.28	57	25	85.00
4 months 150°C	8.34	65	8.29	59	6	66.10
4 months 200°C	8.29	59	8.29	59	0	69.80
4 months 250°C	8.51	88	8.52	88	0	84.00
6 months 150°C	8.37	69	8.29	59	10	72.70
6 months 200°C	8.39	72	8.38	72	0	69.00
6 months 250°C	8.53	90	8.53	90	0	85.60
12 months 150°C	8.22	51	8.22	51	0	72.80
12 months 200°C	8.38	70	8.38	70	0	86.50
12 months 250°C	8.52	88	8.52	88	0	98.20

% Tot. Sm. = total percentage of smectite; % LC. Sm. = percentage of low-charge smectite; % HC. Sm. = percentage of high-charge smectite.

https://doi.org/10.1346/CCMN.1990.0380411 Published online by Cambridge University Press

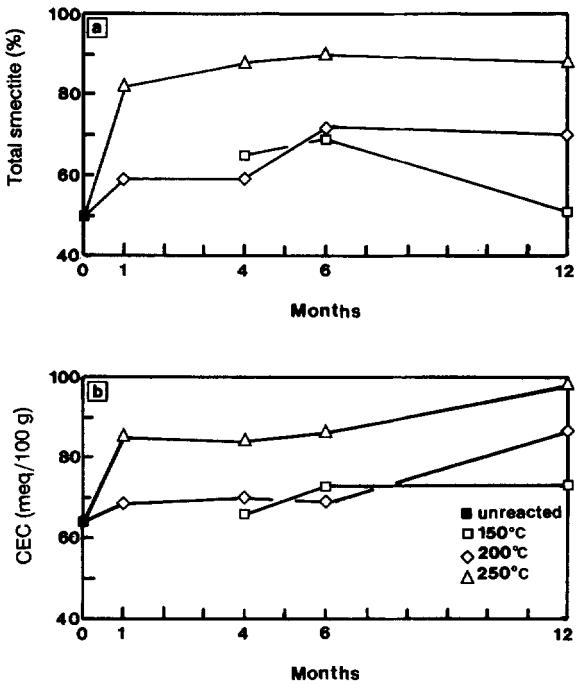

Figure 7. (a) Plots of percentage of total smectite in the mixed-layer kaolinite/smectite estimated from the d(001/002) values as a function of temperatures and run durations. (b) Plots of cation-exchange capacities of bulk clay material as a function of temperatures and run durations.

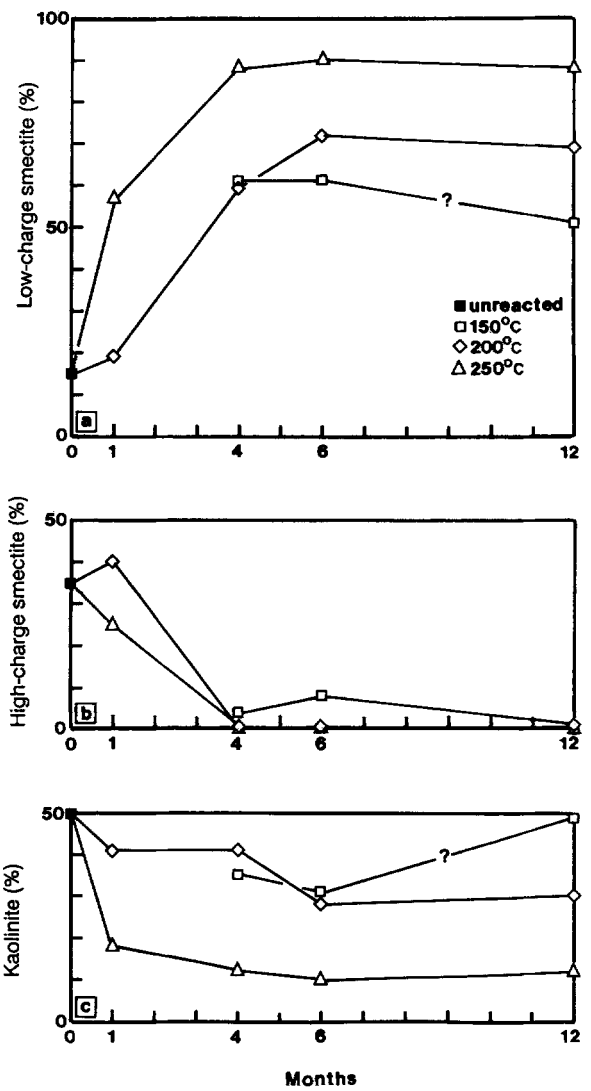

Figure 8. Plots of percentage of component in the mixed-layer kaolinite/smectite as a function of temperatures and run durations. (a) Percentage of low-charge smectite; (b) percentage of high-charge smectite; (c) percentage of kaolinite.

proportion obtained after 4-month reaction, with a maximum at about 90% for the 12 month-250°C run.

The 12 month-250°C XRD pattern (Mg-EG) recorded with the linear detector (Figure 5b) shows a 3.38-Å additional reflection, which can be assigned to the composite $002_{kaolinite}/005_{smectite}$ reflection of a glycolated K/S, containing 10% kaolinite layers (Reynolds, 1980), in good agreement with the proportion of total smectite (88%) determined using the d(001/002) value.

The hydrothermal run at 200°C gave a similar evolutionary trend, but stabilization of the total smectite proportions was obtained only after longer runs (6 months) and gave lower maximum values (about 70%) than those obtained for the 250°C runs.

The 150°C experiments were similar to the 200°C runs for runs as long as 6 months (69% total smectite), but the 12-month experiment showed an unexplained decrease in the total smectite proportion, to the 50% initial content of the unreacted sample.

Figure 7b, a plot of CEC (63.80 meq/100 g for the unreacted sample) vs. time and temperature shows the same evolutionary trend, i.e., a strong increase in the first month of treatment (85.00 meq/100 g at 250°C) and a more gradual increase for longer runs. The CEC values after 12-month reaction depended on temperature, i.e., 72.80, 86.50, and 98.20 meq/100 g at 150°, 200°, and 250°C, respectively. The particular decrease in the smectite proportion observed after the 12-month 150°C reaction did not match with the CEC plateau and can be regarded as inconsistent XRD data, probably resulting from sample heterogeneity.

The proportions of low-charge and high-charge smectite estimated from the XRD data are given in Table 3. Figure 8, a plot of component proportions in the K/S vs. time and temperature, shows that the smectite component in the K/S, originally consisting of 15% low-charge and 35% high-charge layers, converted progressively with time and temperature to low-charge smectite through high-charge smectite and kaolinite destabilization. The reaction reached completion with

https://doi.org/10.1346/CCMN.1990.0380411 Published online by Cambridge University Press

Table 4. Electron microprobe analyses (wt. %) of the clay material reacted at 250°C for 4 months.

Bulk chemical analyses											
											Mean
SiO_2	58.34	56.19	57.58	58.90	57.61	57.60	58.39	58.91	58.13	58.82	58.05
Al_2O_3	26.83	26.65	28.32	26.46	27.90	26.97	26.21	26.39	25.92	26.22	26.79
MnO	—	0.32	0.17	0.50	0.33	0.17	0.16	—	—	—	0.16
MgO	0.86	0.74	0.67	0.47	0.48	0.66	0.95	0.47	1.04	0.95	0.73
CaO	2.70	2.78	2.30	2.43	2.56	2.30	2.70	2.30	2.95	2.69	2.57
Na_2O	0.36	0.35	0.22	0.29	0.36	0.29	0.36	0.22	0.29	0.29	0.30
K_2O	0.33	0.65	0.44	0.44	0.22	0.44	0.33	0.44	0.55	0.33	0.42
TiO_2	0.56	0.55	0.57	0.38	0.56	0.75	0.38	0.75	0.56	0.37	0.54
Fe_2O_3	5.59	5.41	4.15	5.55	5.59	6.96	7.66	5.55	6.22	4.15	5.68
Chemical analyses corrected for goethite (% goet.) and hematite (% hem.)											
% Goet.	4.35	4.21	3.26	4.33	4.35	5.42	5.97	4.32	4.84	3.23	4.43
% Hem.	0.17	0.16	0.13	0.17	0.17	0.21	0.23	0.17	0.19	0.12	0.17
SiO_2	58.34	56.19	57.58	58.90	57.61	57.60	58.39	58.91	58.13	58.82	58.05
Al_2O_3	26.83	26.65	28.32	26.46	27.90	26.97	26.21	26.39	25.92	26.22	26.79
MnO	—	0.32	0.17	0.50	0.33	0.17	0.16	—	—	—	0.16
MgO	0.86	0.74	0.67	0.47	0.48	0.66	0.95	0.47	1.04	0.95	0.73
CaO	2.70	2.78	2.30	2.43	2.56	2.30	2.70	2.30	2.95	2.69	2.57
Na_2O	0.36	0.35	0.22	0.29	0.36	0.29	0.36	0.22	0.29	0.29	0.30
K_2O	0.33	0.65	0.44	0.44	0.22	0.44	0.33	0.44	0.55	0.33	0.42
TiO_2	0.56	0.55	0.57	0.38	0.56	0.75	0.38	0.75	0.56	0.37	0.54
Fe_2O_3	1.51	1.46	1.13	1.50	1.51	1.88	2.07	1.50	1.68	1.12	1.54

the complete destabilization of high-charge smectite layers after 4 months at a minimum temperature of 200°C.

Chemical composition of smectite layers. The chemical composition of the smectite layers was studied on the 250°C-fully reacted clay material (no detectable high-charge layers, no discrete kaolinite, and maximum proportions of low-charge smectite layers) for the 4-, 6-, and 12-month runs. Because XRD patterns indicated the total reaction of calcite after 4 months at 250°C and the stability of the iron oxides, the electron microprobe analyses (Tables 4–6) were first corrected only for goethite and hematite; they thus represent the composition of the mixture, K/S + quartz.

The partial reaction of quartz observed at 250°C as

Table 5. Electron microprobe analyses (wt. %) of the clay material reacted at 250°C for 6 months.

Bulk chemical analyses									
									Mean
SiO_2	58.30	55.74	57.09	58.87	58.63	55.48	55.41	56.39	56.99
Al_2O_3	26.73	25.64	27.32	26.26	27.66	26.11	23.93	26.50	26.27
MnO	0.16	0.32	—	—	—	0.02	0.03	0.01	0.07
MgO	0.47	1.00	1.35	0.57	0.67	0.64	0.96	0.74	0.80
CaO	2.35	2.55	2.49	2.56	2.85	2.20	1.99	2.29	2.41
Na_2O	0.64	0.62	1.13	0.29	0.22	0.38	0.16	0.19	0.45
K_2O	0.40	0.34	0.54	0.33	0.45	0.59	0.64	0.59	0.48
TiO_2	0.42	1.28	0.55	0.56	0.76	1.16	0.98	0.70	0.80
Fe_2O_3	5.26	6.81	5.48	7.63	7.04	6.11	5.55	5.44	6.16
Chemical analyses corrected for goethite (% goet.), and hematite (% hem.)									
% Goet.	4.09	5.31	4.27	5.94	5.48	4.76	4.33	4.24	4.80
% Hem.	0.16	0.20	0.16	0.23	0.21	0.18	0.17	0.16	0.18
SiO_2	58.30	55.74	57.09	58.87	58.63	55.48	55.41	56.39	56.99
Al_2O_3	26.73	25.64	27.32	26.26	27.66	26.11	23.93	26.50	26.27
MnO	0.16	0.32	—	—	—	0.02	0.03	0.01	0.07
MgO	0.47	1.00	1.35	0.57	0.67	0.64	0.96	0.74	0.80
CaO	2.35	2.55	2.49	2.56	2.85	2.20	1.99	2.29	2.41
Na_2O	0.64	0.62	1.13	0.29	0.22	0.38	0.16	0.19	0.45
K_2O	0.40	0.34	0.54	0.33	0.45	0.59	0.64	0.59	0.48
TiO_2	0.42	1.28	0.55	0.56	0.76	1.16	0.98	0.70	0.80
Fe_2O_3	1.42	1.84	1.48	2.06	1.90	1.65	1.50	1.47	1.66

https://doi.org/10.1346/CCMN.1990.0380411 Published online by Cambridge University Press

Table 6. Electron microprobe analyses (wt. %) of the clay material reacted at 250°C for 12 months.

Bulk chemical analyses									
									Mean
SiO_2	58.70	58.29	58.28	58.39	57.90	58.32	58.86	59.06	58.17
Al_2O_3	26.51	25.88	26.41	26.83	28.18	27.49	26.52	28.84	27.20
MnO	—	—	0.16	—	—	—	0.33	0.34	0.10
MgO	0.95	1.05	0.76	0.85	1.15	0.86	0.76	0.67	0.88
CaO	2.57	2.44	2.70	2.70	2.31	2.30	2.71	2.58	2.54
Na_2O	0.29	0.15	0.44	0.36	0.29	0.22	0.44	0.51	0.34
K_2O	0.22	0.33	0.55	0.44	0.33	0.22	0.44	0.33	0.36
TiO_2	0.75	0.94	0.56	0.56	0.76	0.75	0.38	0.76	0.58
Fe_2O_3	7.70	7.70	6.92	6.26	7.00	8.41	6.30	6.30	7.07
Chemical analyses corrected for goethite (% goet.) and hematite (% hem.)									
% Goet.	5.99	6.00	5.39	4.87	5.45	6.54	4.90	4.90	5.50
% Hem.	0.23	0.23	0.21	0.19	0.21	0.25	0.19	0.19	0.21
SiO_2	58.70	58.29	58.28	58.39	57.90	58.32	58.86	59.06	58.17
Al_2O_3	26.51	25.88	26.41	26.83	28.18	27.49	26.52	28.84	27.20
MnO	—	—	0.16	—	—	—	0.33	0.34	0.10
MgO	0.95	1.05	0.76	0.85	1.15	0.86	0.76	0.67	0.88
CaO	2.57	2.44	2.70	2.70	2.31	2.30	2.71	2.58	2.54
Na_2O	0.29	0.15	0.44	0.36	0.29	0.22	0.44	0.51	0.34
K_2O	0.22	0.33	0.55	0.44	0.33	0.22	0.44	0.33	0.36
TiO_2	0.75	0.94	0.56	0.56	0.76	0.75	0.38	0.76	0.58
Fe_2O_3	2.08	2.08	1.87	1.69	1.89	2.27	1.70	1.70	1.91

a function of run duration did not allow an accurate estimation of its content by the microprobe analyses. The direct calculation of a structural formula representing the K/S was also not feasible.

The corrected microprobe analyses plotted on the M^+–4Si–R^{2+} diagram in Figure 9 are in line with the 4Si pole (quartz + kaolinite) and intersect the $be_{0.33}$–$mo_{0.33}$ solid solution line; the variable amounts of quartz shifted the chemical compositions towards the 4Si pole, but did not change the slope of the line, i.e., the intersection point on the $be_{0.33}$–$mo_{0.33}$ solid solution.

Thus, the chemical composition of the low-charge smectite component was approached independent of quartz content, using the percentages of beidellite and montmorillonite obtained from the intersected $be_{0.33}$–$mo_{0.33}$ line (Figure 9) and the composition of each end-member. The resulting structural formulae for the 4-, 6-, and 12-month experiments at 250°C are:

(1) 4 months: $(Si_{3.74}\,Al_{0.26})\,O_{10}\,((Al,Fe^{3+})_{1.92}\,R^{2+}{}_{0.08})\cdot(OH)_2M^+{}_{0.33}$.

(2) 6 months: $(Si_{3.76}\,Al_{0.24}\,O_{10}\,((Al,Fe^{3+})_{1.91}\,R^{2+}{}_{0.09})\cdot(OH)_2M^+{}_{0.33}$.

(3) 12 months: $(Si_{3.76}\,Al_{0.24})\,O_{10}\,((Al,Fe^{3+})_{1.91}\,R^{2+}{}_{0.09})\cdot(OH)_2M^+{}_{0.33}$.

These structural formulae are remarkably similar and close to the estimate of low-charge smectite content in the unreacted K/S. The most relevant fact is that the newly formed low-charge smectites preserved the chemical characteristics of their precursors, i.e., intermediate composition between beidellite and mont-

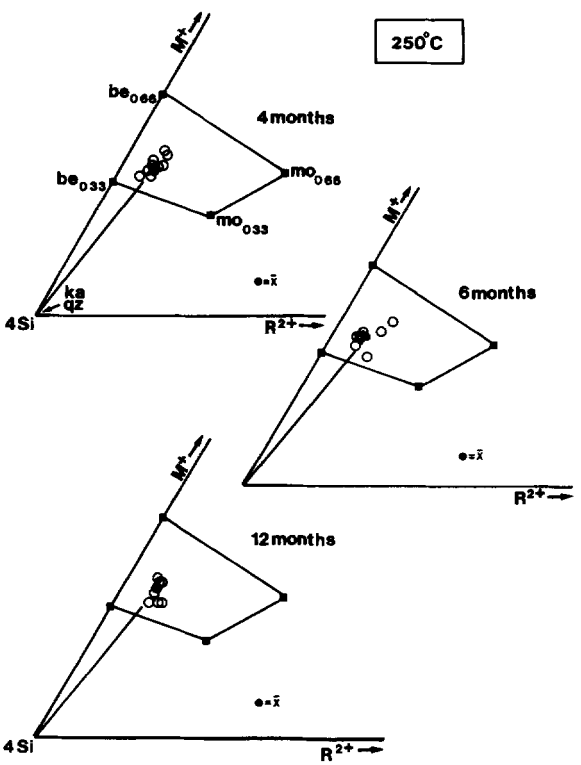

Figure 9. Plots of the corrected microprobe analyses of the reacted clay material at 250°C in the M^+–4Si–R^{2+} diagram; be = beidellite; mo = montmorillonite; $\bar{X}$ = mean value of the microprobe analyses.

https://doi.org/10.1346/CCMN.1990.0380411 Published online by Cambridge University Press

morillonite with simultaneous $Al^{IV} \rightarrow Si^{IV}$ and $R^{2+} \rightarrow Al^{VI}$ substitutions.

Reaction process and kinetics

From the XRD and chemical data, the reactivity of the mixed-layer K/S with time and temperature can be formally written as: High-charge smectite + kaolinite → low-charge smectite. Figure 8 illustrates the kinetics of the high-charge-to-low-charge-smectite conversion and provides the following information on the reaction process: (1) The maximum extent of the reaction was obtained in the 250°C runs. (2) An equilibrium state was reached after 4 months at 250°C, at which time low-charge smectite layers stopped forming and maintained a constant proportion of about 90% for longer runs. (3) At that point in the reaction, the high-charge smectite layers entirely reacted to low-charge layers, whereas the kaolinite layers stopped reacting and maintained a constant proportion of about 10% for longer runs. These observations indicate that the high-charge to low-charge smectite conversion operated rapidly during the first few months and that the completion of the reaction was controlled by the reaction rate of the high-charge smectites with kaolinite.

The proportions of high-charge smectite and kaolinite consumed by the reaction were respectively 35% and 38%, whereas the proportion of newly formed low-charge smectite was 73% (Table 3). Thus, the reaction of the mixed-layer K/S can be written: 0.35 high-charge smectite + 0.38 kaolinite → 0.73 low-charge smectite.

A geochemical balance of the reaction, calculated using the chemical composition of each component, revealed that the reaction of the K/S needed external supplies of silicon (0.69 Si^{4+}) and aluminum (0.12 Al^{3+}). This geochemical balance is well supported by the XRD analyses, which indicated the total dissolution of discrete kaolinite after 4 months at 250°C, together with a partial dissolution of quartz.

CONCLUSION

The high-charge-to-low-charge-smectite reaction apparently can take place in various low-temperature hydrothermal environments with different reactive minerals, i.e., natural I/S hydrothermal alteration (Bouchet *et al.,* 1988) and experimental hydrothermal alteration of K/S. Such reactions induce a marked increase in the cation-exchange capacity for bulk clay material with time and temperature, a result which is of great interest in the use of smectites as backfilling materials in radioactive waste disposals.

This study has raised a new question that must be answered: does pure smectite react in a manner similar to K/S if it is mixed with quartz and kaolinite and subjected to experimental hydrothermal alteration? Additional hydrothermal runs with bentonite are being conducted at the present time to answer this question.

ACKNOWLEDGMENTS

The experimental hydrothermal runs were conducted by the "Commissariat à l'Energie Atomique (C.E.A.)," DRDD/SESD, Fontenay-aux-Roses, France. The information presented in this paper was obtained under contract number F.I.W.-0031 as part of the European Communities (research program on management and disposal of radioactive waste).

REFERENCES

Boles, J. R. and Franks, S. G. (1979) Clay diagenesis in Wilcox sand-stones of southwest Texas: Implication of smectite diagenesis on sandstone cementation: *J. Sed. Petr.* **49,** 55–70.

Bouchet, A., Proust D., Meunier A., and Beaufort, D. (1988) High-charge to low-charge smectite reaction in hydrothermal alteration processes: *Clay Miner.* **23,** 133–146.

Brindley, G. W., Suzuki, T., and Thiry, M. (1983) Interstratified kaolinite/smectites from the Paris Basin: Correlations of layers proportions, chemical compositions and other data: *Bull. Mineral.* **106,** 403–410.

Brown, G. and Brindley, G. W. (1980) X-ray diffraction procedures for clay mineral identification: in *Crystal Structures of Clay Minerals and their X-ray Identification,* G. W. Brindley and G. Brown, eds., Mineralogical Society, London, 339–346.

Čičel, B. and Machajdik, D. (1981) Potassium- and ammonium-treated montmorillonites. I. Interstratified structures with ethylene glycol and water: *Clays & Clay Minerals* **29,** 40–46.

Coulon, H. (1987) Propriétés physicochimiques de sédiments argileux français: Applications au stockage de déchets radioactifs: Thesis, University of Lille, Lille, France, 215 pp.

Eberl, D. (1978) The reaction of montmorillonite to mixed-layer clay: The effect of interlayer alkali and alkaline-earth cations: *Geochim. Cosmochim. Acta* **42,** 1–7.

Eberl, D. and Hower, J. (1976) Kinetics of illite formation: *Geol. Soc. Amer. Bull.* **87,** 1326–1330.

Howard, J. J. (1981) Lithium and potassium saturation of illite/smectite clays from interlaminated shales and sandstones: *Clays & Clay Minerals* **29,** 136–142.

Howard, J. J. and Roy, D. M. (1985) Development of layer charge and kinetics of experimental smectite alteration: *Clays & Clay Minerals* **33,** 81–88.

Hower, J. and Mowatt, T. C. (1966) The mineralogy of illites and mixed-layer illite-montmorillonite: *Amer. Mineral.* **51,** 825–854.

Hower, J., Eslinger, E. V., Hower, M. E., and Perry, E. A. (1976) Mechanism of burial metamorphism of argillaceous sediments: I. Mineralogical and chemical evidence: *Geol. Soc. Amer. Bull.* **87,** 725–737.

Inoue, A., Minato, H., and Utada, M. (1978) Mineralogical properties and occurrence of illite/montmorillonite mixed-layer minerals formed from Miocene volcanic glass in Waga-Omono district: *Clay Sci.* **5,** 123–136.

Inoue, A. and Utada, M. (1983) Further investigations of a conversion series of dioctahedral mica/smectite in the Shinzan hydrothermal alteration area, northeast Japan: *Clays & Clay Minerals* **31,** 401–412.

Jackson, M. L. (1958) *Soil Chemical Analysis,* 3rd ed., Prentice Hall, Englewood Cliffs, New Jersey, 498 pp.

Lucas, J., Trauth, N., and Thiry, M. (1974) Les minéraux argileux des sédiments paléogènes du bassin de Paris. Evolution des smectites et des interstratifiés (7–14): *Bull. Gr. Franç. Argiles* **26,** 245–262.

Meunier, A. and Velde, B. (1989) Solid solutions in I/S mixed-layer minerals and illite: *Amer. Mineral.* **74,** 1106–1112.

Nadeau, P. H. and Bain, D. C. (1986) Composition of some smectites and diagenetic illitic clays and implications for their origin: *Clays & Clay Minerals* **34,** 455–464.

Ramseyer, K. and Boles, J. R. (1986) Mixed-layer illite/smectite in tertiary sandstones and shales, San Joaquin Basin, California: *Clays & Clay Minerals* **34,** 115–124.

Rassineux, F., Beaufort, D., Bouchet, A., Merceron, T., and Meunier, A. (1988) Use of a linear localization detector for X-ray diffraction of very small quantities of clay minerals: *Clays & Clay Minerals* **36,** 187–189.

Reynolds, R. C. (1980) Interstratified clay minerals: in *Crystal Structures of Clay Minerals and their X-ray Identification,* G. W. Brindley and G. Brown, eds., Mineralogical Society, London, 249–303.

Reynolds, R. C. and Hower J. (1970) The nature of interlayering in mixed-layer illite-montmorillonite: *Clays & Clay Minerals* **18,** 25–36.

Roberson, H. E. and Lahann, R. W. (1981) Smectite to illite conversion rates: Effects of solution chemistry: *Clays & Clay Minerals* **29,** 129–135.

Środoń, J. (1980) Precise identification of illite/smectite interstratifications by X-ray powder diffraction: *Clays & Clay Minerals* **28,** 401–411.

Środoń, J., Morgan, D. J., Eslinger, E. V., Eberl, D., and Karlinger, M. R. (1986) Chemistry of illite/smectite and end-member illite: *Clays & Clay Minerals* **34,** 368–378.

Thiry, M. (1981) Sédimentation continentale et altération associées: Calcitisations, ferruginisations et silicifications. Les argiles plastiques du Sparnacien du bassin de Paris: *Sci. Géol. Mém.* **64,** 173 pp.

Thiry, M., Cavelier, C., and Trauth, N. (1977) Les sédiments de l'Eocène inférieur du bassin de Paris et leurs relations avec la paléoaltération de la craie: *Sci. Géol. Bull.* **30,** 113–128.

Velde, B. (1984) Electron microprobe analysis of clay minerals: *Clay Miner.* **19,** 243–247.

Velde, B. and Brusewitz, A. M. (1982) Metasomatic and non metasomatic low-grade metamorphism of Ordovician metabentonites in Sweden: *Geochim. Cosmochim. Acta* **46,** 447–452.

Voinovitch, I. A., Debras-Guédon, J., and Louvrier, J. (1962) *L'Analyse des Silicates:* I. A. Voinovitch, ed., Hermann, Paris, 510 pp.

(Received 13 April 1989, accepted 15 February 1990; Ms. 1903)